White Rose Research Online

eprints@whiterose.ac.uk
https://eprints.whiterose.ac.uk
Universities of Leeds, Sheffield and York

Deposited via The University of Sheffield.

White Rose Research Online URL for this paper:
https://eprints.whiterose.ac.uk/id/eprint/163033/

Version: Accepted Version

Article:
Blackburn, L.R., Sun, S.K., Gardner, L.J. et al. (2020) Influence of transition metal charge compensation species on phase assemblage in zirconolite ceramics for Pu immobilisation. MRS Advances, 5 (1-2). pp. 93-101. ISSN: 2059-8521

https://doi.org/10.1557/adv.2020.100

This article has been published in a revised form in MRS Advances https://doi.org/10.1557/adv.2020.100. This version is free to view and download for private research and study only. Not for re-distribution, re-sale or use in derivative works. © Materials Research Society 2020.

Reuse
This article is distributed under the terms of the Creative Commons Attribution-NonCommercial-NoDerivs (CC BY-NC-ND) licence. This licence only allows you to download this work and share it with others as long as you credit the authors, but you can't change the article in any way or use it commercially. More information and the full terms of the licence here: https://creativecommons.org/licenses/

Takedown
If you consider content in White Rose Research Online to be in breach of UK law, please notify us by emailing eprints@whiterose.ac.uk including the URL of the record and the reason for the withdrawal request.

UNIVERSITY OF LEEDS
University of Sheffield
UNIVERSITY of York

MRS Advances

Influence of Transition Metal Charge Compensation Species on Phase Assemblage in Zirconolite Ceramics for Pu Immobilisation

L.R. Blackburn[1], S.K. Sun[1], L.J. Gardner[1], E.R. Maddrell[2], M.C. Stennett[1], N.C. Hyatt[1]

[1]*Immobilisation Science Laboratory, University of Sheffield, Department of Materials Science and Engineering, Sir Robert Hadfield Building, Mappin Street, S13JD, UK*

[2]*National Nuclear Laboratory, Workington, Cumbria, CA14 3YQ, UK*

ABSTRACT

Immobilisation of Pu in a zirconolite matrix ($CaZrTi_2O_7$) is a viable pathway to disposition. A-site substitution, in which Pu^{4+} is accommodated into the Ca^{2+} site in zirconolite, coupled with sufficient trivalent M^{3+}/Ti^{4+} substitution (where M^{3+} = Fe, Al, Cr), has been systematically evaluated using Ce^{4+} as a structural analogue for Pu^{4+}. A broadly similar phase assemblage of zirconolite-2M and minor perovskite was observed when targeting low levels of Ce incorporation. As the targeted Ce fraction was elevated, secondary phase formation was influenced by choice of M^{3+} species. Co-incorporation of Ce/Fe resulted in the stabilisation of a minor Ce-containing perovskite phase at high wasteloading, whereas considerable phase segregation was observed for Cr^{3+} incorporation. The most favourable substitution approach appeared to be achieved with the use of Al^{3+}, as no perovskite or free CeO_2 was observed. However, high temperature treatments of Al containing specimens resulted in the formation of a secondary Ce-containing hibonite phase.

INTRODUCTION

The United Kingdom Nuclear Decommissioning Authority (NDA) is responsible for the safe and long term management of waste derived from the reprocessing of spent fuel from civil power generation [1]. Reprocessing of nuclear fuels in the UK has resulted in a significant stockpile of civil separated Pu, forecast to reach 140 teHM [2]. The default strategy for this material is continuous interim storage (subject to periodic repackaging) at the Sellafield site. However, NDA is currently in the process of refining the 'credible options' framework, exploring potential reuse and disposal options for UK stockpiled Pu. The UK Government has

placed preference on the fabrication of $(U/Pu)O_2$ mixed oxide fuels (MOX) for use in a fleet of civil light water reactors [3]. Yet, some portion of the stockpile may not meet the requirements for the manufacture of MOX fuel due to degradation and contamination, hence, prompt immobilisation and disposal in a suitable glass or ceramic matrix is considered a viable and proliferation resistant management strategy for this material.

Alkali borosilicate glass wasteforms are currently operational for the immobilisation of chemically heterogeneous calcines derived from aqueous reprocessing operations, however, ceramic matrices are considered a more suitable option for wastes with a high actinide fraction. Zirconolite, with ideal composition $CaZrTi_2O_7$, is a naturally occurring titanate phase that is the candidate host for Pu in the UK [4]. Natural zirconolites have demonstrated excellent resistance to extensive weathering and self-irradiation over geological timescales (10^9 years), whilst retaining significant actinide inventories (in some instances approximately 20 wt. %). In the ideal zirconolite-2M structure, planes of Ca^{2+} and Zr^{4+} (8 and 7-fold oxygen coordinated respectively) are arranged between sheets of Ti arranged in hexagonal tungsten bronze type (HTB) motifs. The Ca/Zr layers and HTB units alternate parallel to (001), whilst HTB layers at z = 0.25 and z = 0.75 are orientated by a 180˚ rotation, along the [130] direction [5]. The nomenclature '2M' refers to the two layer repeating sequence forming the unit cell. With reference to the prototypical composition $CaZr_xTi_{3-x}O_7$, the zirconolite-2M polytype is found to be stable over the compositional range $0.83 < x < 1.33$ [6]. Further zirconolite polytypes (*e.g.* 4M, 3T, 3O) have been reported, the formation these polytypes, is postulated to be controlled by the level of targeted Ln^{3+}/An^{4+} incorporation, processing temperature and target site [7–9]. Pu^{4+} can enter the zirconolite lattice *via* solid solution with either Ca^{2+} and/or Zr^{4+} sites, which can create charge imbalance. Co-substitution of a lower valence cation such as Al^{3+} on the Ti^{4+} sites is necessary for Ca^{2+} substitution, in order to maintain isovalence across the structure. In the present work, we aim to systematically evaluate the influence of trivalent charge compensation species Fe^{3+}, Cr^{3+} and Al^{3+} on zirconolite phase evolution. In this instance, Ce^{4+} is used as a structural surrogate for Pu^{4+}.

EXPERIMENTAL

A series of zirconolite ceramics were batched according to composition $Ca_{1-x}Ce_xZrTi_{2-2x}M_{2x}O_7$ ($0.05 \leq x \leq 0.35$, 0.05 increments) with M^{3+} = Cr/Al/Fe as a charge balancing species. $CaTiO_3$, ZrO_2, CeO_2, M_2O_3, and TiO_2 (Alfa Aesar, 99.9% purity, trace metals basis) were batched according to nominal stoichiometry and mixed by high speed planetary milling (Fritsch P7, 400 rpm, 20 min, IPA carrier fluid). Approximately 0.3 g of homogenised precursor material was pressed into the walls of a 10 mm hardened steel die and pressed under 3 t uniaxial pressure. Green bodies were sintered in air at 1350 ˚C for 20 h. Specimens were prepared for powder X-ray diffraction using a Bruker D2 Phaser, fitted with Lynxeye position sensitive detector, using a Cu Kα source (λ = 1.5418 Å, Ni filter). Identified phases were refined using the Rietveld method. Samples were mounted in cold setting resin and polished to a 1 μm finish prior to SEM analysis using a Hitachi TM3030 scanning electron microscope, operating at 15 kV with a working distance of approximately 8 mm. Semi-quantitative analysis was performed using a Bruker Quantax Energy Dispersive X-ray Spectrometer (EDS).

RESULTS AND DISCUSSION

$Ca_{1-x}Ce_xZrTi_{2-2x}Fe_{2x}O_7$

When targeting a nominal composition x = 0.10, zirconolite-2M was identified as the dominant crystalline phase (space group *C2/c*). This was determined by powder X-ray diffraction measurements (**Fig. 1**), and later confirmed by zone axis electron diffraction techniques (not shown). Intense reflections indicative of prototypical zirconolite-2M were observed alongside a minor perovskite phase, nominally $CaTiO_3$, identified by diagnostic reflection 2θ = 33.1˚. This was consistent with the microstructure observed in SEM analysis of well-sintered regions (**Fig. 2**). Perovskite clusters were observed to be distributed throughout the ceramic, observed as darker grey particulates in **Fig. 2**. At x = 0.10, perovskite comprised 1.72 ± 0.24 wt. % of the overall phase assemblage. EDS analysis also demonstrated partial retention of Ce and Fe within the perovskite phase whilst zirconolite-2M exhibited an average composition in good agreement with the nominal stoichiometry. This was confirmed by semi-quantitative EDS measurements (**Table 1**). As the targeted level of Ce/Fe incorporation was elevated, no significant phase separation was observed. When the nominal concentration of Ce was elevated to x = 0.35, perovskite remained present as a secondary phase, accounting for 3.46 ± 0.60 wt. % of the overall phase assemblage. No free CeO_2 or Fe_2O_3 oxides were readily identified by XRD analysis (**Fig. 3**) or by SEM analysis, where only a matrix of zirconolite-2M with considerable perovskite was present (**Fig. 4**).

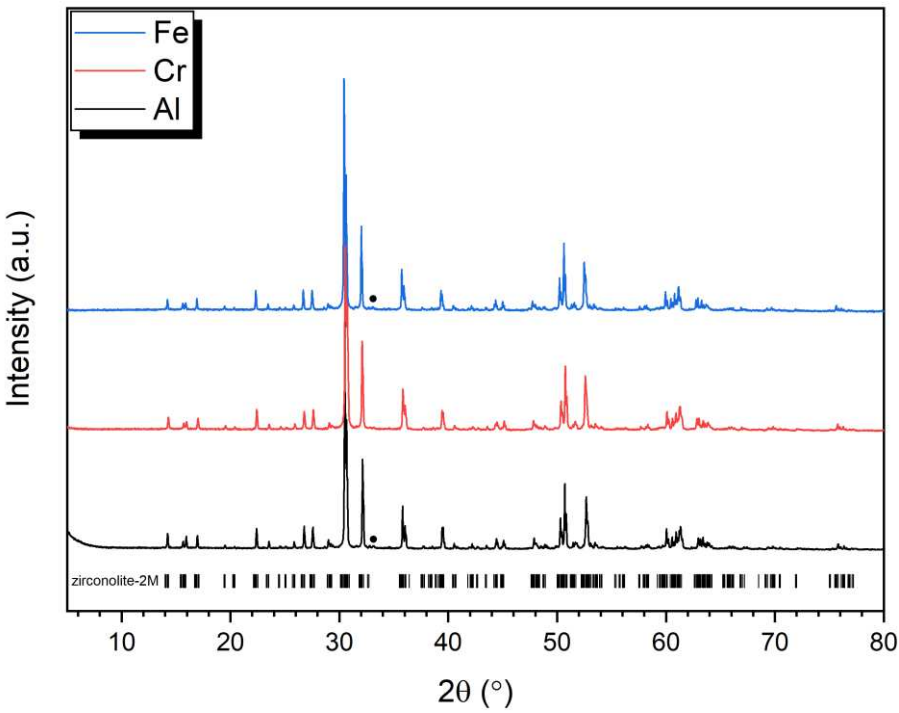

Fig. 1) Powder X-ray diffraction measurements for $Ca_{0.90}Ce_{0.10}ZrTi_{1.80}M_{0.20}O_7$ where M^{3+} = Al/Fe/Cr. Nominal zirconolite-2M reflections are indicated. Minor perovskite inclusions are indexed by (●).

$Ca_{1-x}Ce_xZrTi_{2-2x}Cr_{2x}O_7$

Single phase zirconolite-2M was attained when targeting nominal stoichiometry $Ca_{0.90}Ce_{0.10}ZrTi_{1.80}Cr_{0.20}O_7$, with no perovskite indexed by powder XRD measurements (**Fig. 1**). This was confirmed by zone axis electron diffraction measurements. A homogeneous matrix was observed when viewing polished surfaces (**Fig. 2**). It was, however, noted that all specimens doped with chromium formed with considerable porosity, with respect to the Fe/Al samples (**Fig. 2** and **Fig. 5**). The observed composition is in general agreement with the nominal stoichiometry – **Table 1**. No perovskite was observed when targeting low Ce/Cr substitution ($x < 0.15$). SEM evidenced several secondary phases as the concentration of Ce/Cr was further increased; XRD measurements evidenced free Cr_2O_3 and perovskite for $x = 0.35$ (**Fig. 3**). These phases comprised 2.50 ± 0.26 wt. % and 3.22 ± 0.33 wt. % of the overall phase assemblage, respectively. EDS analysis confirmed co-partitioning of some Ce and Cr in the perovskite phase at $x = 0.35$. SEM analysis also revealed minor ZrO_2 and CeO_2 to be present in the microstructure, these were not readily evidenced by powder XRD due to overlap of diagnostic peaks. Typical phase segregation and elemental distribution for $Ca_{0.65}Ce_{0.35}ZrTi_{1.30}Cr_{0.70}O_7$ is shown in **Fig. 5**.

Table 1) Average zirconolite-2M compositions determined from semi-quantitative EDS analysis (normalized to seven oxygen units).

	Observed Average Composition		
Nominal composition	$Ca_{1-x}Ce_xZrTi_{2-2x}Al_{2x}O_7$	$Ca_{1-x}Ce_xZrTi_{2-2x}Fe_{2x}O_7$	$Ca_{1-x}Ce_xZrTi_{2-2x}Cr_{2x}O_7$
x = 0.10	$Ca_{0.94(4)}Ce_{0.08(4)}Zr_{0.95(7)}Ti_{1.82(6)}Al_{0.22(4)}O_7$	$Ca_{0.95(4)}Ce_{0.07(2)}Zr_{0.93(8)}Ti_{1.86(8)}Fe_{0.19(3)}O_7$	$Ca_{0.94(5)}Ce_{0.07(1)}Zr_{0.93(12)}Ti_{1.89(28)}Cr_{0.17(3)}O_7$
x = 0.35	$Ca_{0.78(6)}Ce_{0.31(10)}Zr_{0.97(10)}Ti_{1.49(10)}Al_{0.44(7)}O_7$	$Ca_{0.69(12)}Ce_{0.28(6)}Zr_{1.04(11)}Ti_{1.41(11)}Fe_{0.57(7)}O_7$	$Ca_{0.68(7)}Ce_{0.30(4)}Zr_{1.01(10)}Ti_{1.46(8)}Cr_{0.52(6)}O_7$

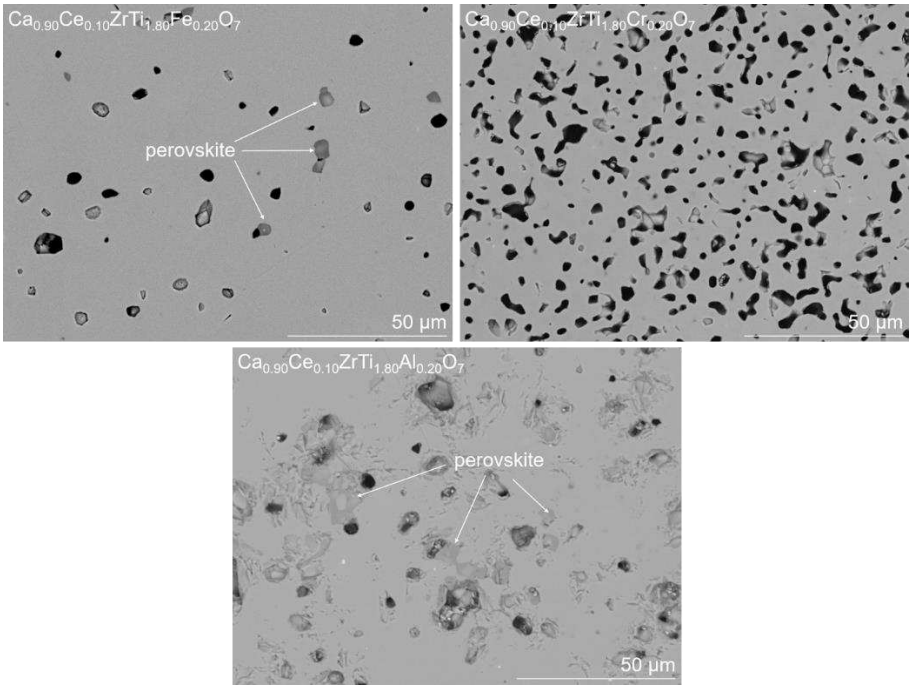

Fig. 2) Representative backscattered electron micrographs for specimens with nominal composition x = 0.10.

$Ca_{1-x}Ce_xZrTi_{2-2x}Al_{2x}O_7$

Intense reflections indicative of prototypical zirconolite-2M were observed for nominal stoichiometry $Ca_{0.90}Ce_{0.10}ZrTi_{1.80}Al_{0.20}O_7$, alongside a minor perovskite phase as indexed in **Fig. 1**, comprising 1.72 ± 0.24 wt. % of the phase assemblage. Electron diffraction techniques inferred that zirconolite remained present in the 2M polytype. The phase assemblage identified by powder XRD was confirmed by SEM analysis of the polished surfaces to be a matrix of zirconolite-2M, with minor Al_2O_3 present at high wasteloading. **Fig. 2** displays a dense matrix of zirconolite-2M, with perovskite inclusions evidenced by variation in backscattered electron contrast, with brighter grains indicating overall greater Ce fraction. EDS analysis confirmed Ce accommodation in the perovskite phase, suggesting the formation of Ce^{3+}. As the Ce/Al fraction was elevated to x = 0.35, the separation of a secondary Al_2O_3 phase was observed, this is evidenced by reflections at approximately 2θ = 25.6˚ and 35.2˚, accounting for 4.01 ± 0.54 wt. % of the phase assemblage. In contrast to the Fe and Cr systems, no perovskite was observed in the microstructure when targeting maximum Ce concentration x = 0.35. A representative microstructure for $Ca_{0.65}Ce_{0.35}ZrTi_{1.60}Al_{0.40}O_7$ is displayed in **Fig. 6**, with a minor amount of $(Ce,Zr)O_2$ present (< 1 wt. %). Whilst perovskite is a common accessory phase in the fabrication of zirconolite specimens (attributed to the partial formation of Ce^{3+}), perovskite has a markedly lower resistance to hydrothermal alteration with respect to zirconolite [10,11]. Therefore, the accommodation of Ce within the Ca^{2+} site of zirconolite-2M may be best achieved *via* the co-partitioning of Al^{3+} on the Ti^{4+} site, in order to inhibit perovskite formation. It was however noted, in separate trials on the same precursor, that a sintering regime in which 1450 ˚C was reached, resulted in the crystallization of a Ce-bearing hibonite phase (ideally $CaAl_{12}O_{19}$). This was not evidenced in the current work, as the formation temperature of nominal $CaAl_{12}O_{19}$ is quoted to be approximately 1500 ˚C [12].

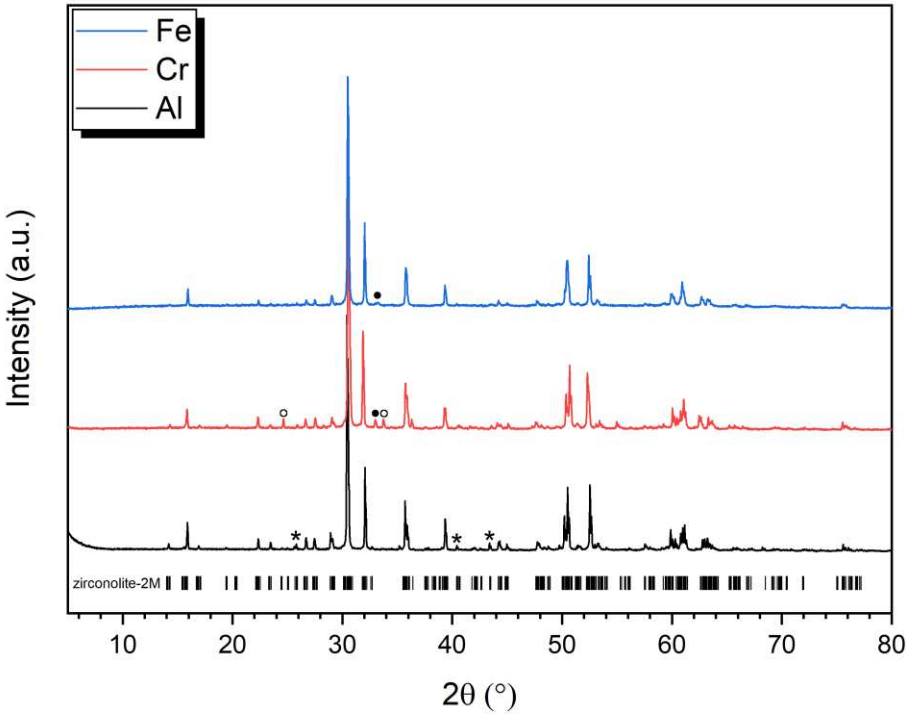

Fig. 3) Powder X-ray diffraction measurements for $Ca_{0.65}Ce_{0.35}ZrTi_{1.30}M_{0.70}O_7$ where M^{3+} = Al/Fe/Cr. Nominal zirconolite-2M reflections are indicated. Minor perovskite and Cr_2O_3 inclusions are indexed by (●) and (o) respectively. Al_2O_3 phases are denoted by (*)

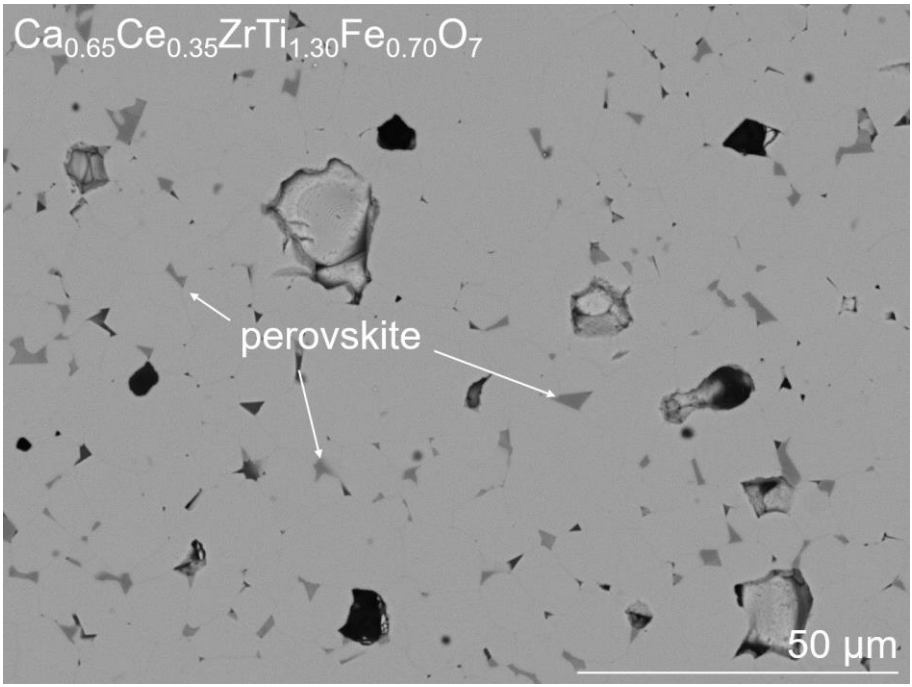

Fig. 4) Backscattered electron micrograph for Fe-doped specimen with nominal x = 0.35 composition.

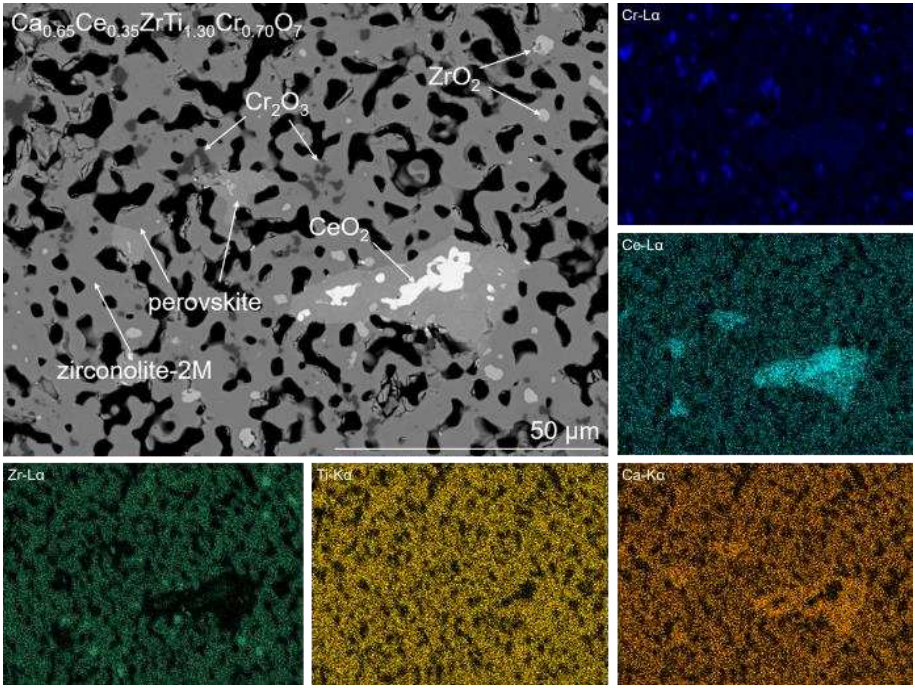

Fig. 5) Representative BSE micrograph and corresponding EDS maps for Ce/Cr doped specimen with nominal composition $Ca_{0.65}Ce_{0.35}ZrTi_{1.30}Cr_{0.70}O_7$.

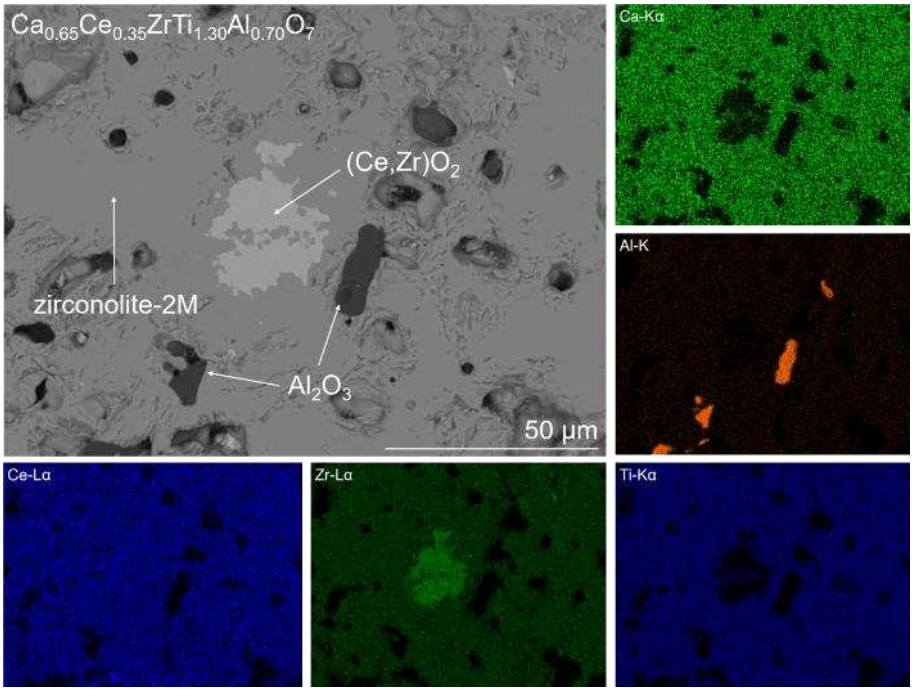

Fig. 6) Representative BSE micrograph and corresponding EDS maps for Ce/Al doped specimen with nominal composition $Ca_{0.65}Ce_{0.35}ZrTi_{1.30}Al_{0.70}O_7$.

CONCLUSIONS

Zirconolite ceramics are under consideration as a host matrix for the immobilisation of civil UK Pu that does not meet the requirements for MOX fuel fabrication. Pu^{4+} may enter the zirconolite system *via* $Ca_{1-x}Pu_xZrTi_{2-2x}M_{2x}O_7$ with the co-substitution of some M^{3+} trivalent species to provide charge balance. The prevailing phase assemblage was likely controlled by size constraints between Ti^{4+} and M^{3+} sites, alongside thermodynamic considerations. When targeting relatively low Ce incorporation (*i.e.* $x \geq 0.15$) a broadly similar phase assemblage and microstructure was observed when utilizing Fe/Cr/Al charge compensation species. When attempting to a substitute high Ce fraction ($x = 0.35$), Fe charge compensation favored the formation of a minor Ce-containing perovskite phase, whilst considerable phase separation and perovskite inclusions were observed for Cr^{3+} samples. Specimens formed with Al^{3+} produced the most favorable phase assemblage due to the lack of secondary $CaTiO_3$. The suppression of secondary perovskite phases is desirable, given the lower aqueous durability of this phase with respect to the target zirconolite phase. Based on the current work, Al^{3+} and Fe^{3+} charge compensation produced wasteforms with the lowest accessory perovskite fraction, and may therefore be considered superior candidates for charge balance than Cr^{3+}. Considerations with respect to temperature should, however, be noted. These results are promising towards the refinement and evaluation of a single phase ceramic host for Pu.

ACKNOWLEDGEMENTS

We are grateful for financial support from the Nuclear Decommissioning Authority and EPSRC under grant numbers EP/M026566/1, EP/S01019X/1, EP/N017870/1 and

EP/R511754/1. This research utilized the MIDAS facility at the University of Sheffield established with financial support from the Department for Energy and Climate Change, now incorporated within the Department for Business, Energy and Industrial Strategy.

References

1. Nuclear Decommissioning Authority, *NDA Plutonium Options* (2008).
2. N.C. Hyatt, Energy Policy **101**, 303 (2017).
3. Nuclear Decommissioning Authority, *NDA Plutonium Topic Strategy: Credible Options Technical Summary* (2009).
4. M.C. Stennett, N.C. Hyatt, M. Gilbert, F.R. Livens, and E.R. Maddrell, in *Mater. Res. Soc. Symp. Proc.* (2008), pp. 1–6.
5. A.A. Coelho, R.W. Cheary, and K.L. Smith, J. Solid State Chem. **129**, 346 (1997).
6. B.M. Gatehouse, I.E. Grey, R.J. Hill, and H.J. Rossell, Acta Cryst. **B37**, 306 (1981).
7. B.M. Clark, S.K. Sundaram, and S.T. Misture, Sci. Rep. **7**, 2 (2017).
8. S. Ma, S. Ji, C. Liao, C. Liu, K. Shih, and W. He, Ceram. Int. **44**, 15124 (2018).
9. N. V. Zubkova, N. V. Chukanov, I. V. Pekov, B. Ternes, W. Schüller, D.A. Ksenofontov, and D.Y. Pushcharovsky, Zeitschrift Fur Krist. - Cryst. Mater. **233**, 463 (2018).
10. K.L. Smith, G.R. Lumpkin, M.G. Blackford, R.A. Day, and K.P. Hart, J. Nucl. Mater. **190**, 287 (1992).
11. S. Myhra, H.E. Bishop, J.C. Rivière, and M. Stephenson, J. Mater. Sci. **22**, 3217 (1987).
12. J. Li, E.A. Medina, J.K. Stalick, A.W. Sleight, and M.A. Subramanian, Prog. Solid State Chem. **44**, 107 (2016).